SOLAR WIND SPUTTERING EFFECTS IN THE MARTIAN ATMOSPHERE*

C. C. WATSON and P. K. HAFF

A. W. Wright Nuclear Structure Laboratory†
Yale University, New Haven, Connecticut 06520

and

W. K. Kellogg Radiation Laboratory
California Institute of Technology, Pasadena, California 91125

ABSTRACT

A Monte Carlo simulation of the sputtering of the upper atmosphere of Mars by the solar wind has been performed. The calculated sputtering yields imply loss rates (molecules/cm^2-sec escaping the planet) for carbon dioxide, carbon, and oxygen of $R_{CO_2} = 2.6 \times 10^6/cm^2$-sec, $R_C = 6.6 \times 10^5/cm^2$-sec, and $R_O = 7.7 \times 10^5/cm^2$-sec. The total mass loss by sputtering is only ~ 10% of that due to chemical and photo-chemical processes, but sputtering provides a major exospheric sink for carbon. Because of diffusive separation of lighter elements and isotopes and because the gravitational binding energy is proportional to the mass, the erosion process described here preferentially removes the lighter components of the atmosphere. Solar wind sputtering thus competes favorably with other erosion mechanisms in generating substantial fractionation effects. Calculations based on a Monte Carlo simulation suggest that for a model atmosphere, 97% of the N_2 and 33% of the CO_2 originally present may have been sputtered away over 4.5×10^9 y. In the same length of time the $^{15}N/^{14}N$ isotopic ratio for the bulk atmosphere would have increased by a factor of 1.7.

---

*Supported in part by the Department of Energy [EY76-C-02-3074, EX76-G-03-1305], the National Aeronautics and Space Administration [NGR 05-002-333], and the National Science Foundation [PHY76-83685].

†Permanent address.

ONE OF THE LIME AID PREPRINT SERIES
IN NUCLEAR GEOPHYSICS AND COSMOCHEMISTRY

January 1979

SOLAR WIND SPUTTERING EFFECTS IN THE MARTIAN ATMOSPHERE*

C. C. WATSON and P. K. HAFF

A. W. Wright Nuclear Structure Laboratory†
Yale University, New Haven, Connecticut 06520

and

W. K. Kellogg Radiation Laboratory
California Institute of Technology, Pasadena, California 91125

ABSTRACT

A Monte Carlo simulation of the sputtering of the upper atmosphere of Mars by the solar wind has been performed. The calculated sputtering yields imply loss rates (molecules/cm^2-sec escaping the planet) for carbon dioxide, carbon, and oxygen of $R_{CO_2} = 2.6 \times 10^6/cm^2$-sec, $R_C = 6.6 \times 10^5/cm^2$-sec, and $R_O = 7.7 \times 10^5/cm^2$-sec. The total mass loss by sputtering is only ~ 10% of that due to chemical and photo-chemical processes, but sputtering provides a major exospheric sink for carbon. Because of diffusive separation of lighter elements and isotopes and because the gravitational binding energy is proportional to the mass, the erosion process described here preferentially removes the lighter components of the atmosphere. Solar wind sputtering thus competes favorably with other erosion mechanisms in generating substantial fractionation effects. Calculations based on a Monte Carlo simulation suggest that for a model atmosphere, 97% of the N_2 and 33% of the CO_2 originally present may have been sputtered away over 4.5×10^9 y. In the same length of time the $^{15}N/^{14}N$ isotopic ratio for the bulk atmosphere would have increased by a factor of 1.7.

*Supported in part by the Department of Energy [EY76-C-02-3074, EX76-G-03-1305], the National Aeronautics and Space Administration [NGR 05-002-333], and the National Science Foundation [PHY76-83685].

†Permanent address.

ONE OF THE LIME AID PREPRINT SERIES
IN NUCLEAR GEOPHYSICS AND COSMOCHEMISTRY
January 1979

INTRODUCTION

Energetic solar wind protons and α particles, upon entering the upper atmosphere of Mars, initiate collisional cascades among the atmospheric molecules, predominantly CO_2 and N_2, which result in the escape of atoms and molecules from the Martian gravitational field (Haff, et al., 1978). This sputtering effect is investigated as a mechanism of atmospheric mass loss by means of a Monte Carlo calculation of the appropriate sputtering yields. Section I summarizes the input assumptions of our simulation and discusses their motivation and probable effects on the results. In Section II we outline the calculational technique briefly and then present results. The implications of the calculated yields for atmospheric mass loss are discussed in Section III and a comparison is made to other loss mechanisms. The role of sputtering in determining the compositional history of the Martian atmosphere, including isotopic fractionations, is analyzed in Section IV. An appendix contains some remarks on the accuracy and reliability of our results.

I.

We have considered model atmospheres which are isothermal, with plane isobaric surfaces. The following discussion is primarily concerned with the CO_2 component, but the same considerations apply qualitatively to the N_2 calculations. Effects of curvature of the atmosphere were neglected since the lateral dimension of the cascades was only ~100 km, compared to the planetary radius $R_{Mars} = 3.35 \times 10^3$ km. The density of an atmosphere in

thermal equilibrium varies with altitude as $\rho(z) = \rho_o e^{-z/H}$ (H = scale height). Data obtained by the Viking Landers (Nier and McElroy, 1976, 1977) indicated that for the altitudes with which we are primarily concerned, 100 km < z < 200 km, this distribution can represent the actual density to within a few percent, sufficient for our purposes. The values $\rho_o = 1.2 \times 10^{16}/cm^3$ (not the surface density) and H = 10.0 km, used for the CO_2 sputtering calculation, were determined from the VLI measurements. The same data indicate that at 160 km the atmosphere is ~87% CO_2, with N_2, CO and Ar being the most abundant remaining components. Thus our assumption of 100% CO_2 overestimates the yields by 10-15%.

The solar wind protons were assumed to be monoenergetic, E = 1 keV, and to enter the atmosphere normally. Measurements show that at least during the quiet periods of solar activity the energy distribution of these protons is fairly sharply peaked at 1 keV (Brandt, 1970). The assumption of normal incidence is more uncertain since the characteristics of the solar wind flow about Mars are poorly known. It has in fact been calculated that, due to the shielding effects of the ionosphere, the solar wind may not penetrate below 175-155 km at the subsolar point (Spreiter, et al., 1970). If this distance significantly exceeds the critical height h_c the solar wind may be diverted around the planet in nearly collisionless flow so that little absorption by the atmosphere occurs. However, at distances comparable to or somewhat in excess of h_c, the relatively rare proton-molecule collisions

which do occur (see Fig. 4 below) are efficient at producing sputtered particles. Any ionospheric deflection would greatly increase the proton path length in this region with a corresponding increase in the sputtering yield. For example, if even a tenth of the deflected flux were to follow a roughly circular path at an altitude of 190 km or less, the resulting mass loss is comparable to that resulting from normal incidence. Similar enhancements due to oblique incidence are well known for ion bombardment of solids. Because of the uncertainties in the flow pattern we have not included this effect in our numerical results. Note that shielding effects may not be constant in time, and occasional transitions from nearly collisionless to absorptive flow may occur spontaneously due to the known variability of the solar wind (Spreiter, et al., 1970).

Variations in the sputtering yield due to induced changes in the incident proton energy spectrum would be expected to be relatively minor since the yield is not a strong function of energy. Variations arising from changes in the flow pattern as discussed above can be scaled roughly from the present results when the nature of the flow has been established.

In the present paper the numerical results are based upon the assumption that the solar wind is incident directly onto the atmosphere. Since the calculated mass loss rates are large, and inasmuch as the phenomenon of particle-induced atmospheric erosion may occur elsewhere in the solar system, we

proceed to present details of proton induced cascades in the upper Martian atmosphere. Since the solar wind consists of ~5% alpha particles with energy $E \approx 4$ keV (Brandt, 1970) their sputtering yield was also calculated, subject to the same assumptions.

Although the $H^+ + CO_2$ collisions clearly have many open exit channels, most of these are not important in sputtering because the momentum transfer is small. It is the direct atom-atom collisions which are most significant here, namely

$$H^+ + CO_2 \rightarrow H^+ + C + O_2,$$

or $$H^+ + CO_2 \rightarrow H^+ + O + CO$$

or $$H^+ + CO_2 \rightarrow H^+ + CO_2$$

for collisions leading to sputtering. As discussed below, the first two reactions are the most important in the present context. The exact electronic configuration of the reaction products here is not of direct importance to our calculations since ion-atom (or ion-molecule) cross sections depend only weakly on the charge state of the ion. Excitation and ionization processes, however, are significant to the extent that they reduce the energy available for the production of secondaries. Such loss mechanisms were not built into our model, but an estimate of their effect is made in the appendix. Each $H^+ + CO_2$ break-up collision was treated as being between an H^+ and a free C or O atom. If the energy transfer, T, was greater than a critical energy taken to be the sum of the gravitational binding energy of the atom and its dissociation energy, D, then the CO_2 was assumed to break-up with the possibility of one fragment of energy T-D escaping the planet. This critical energy is 7.5 eV for O and 12.5 eV for C.

Smaller energy transfers do not contribute to sputtering.

The model of complete break-up obtains for the following reasons. Calculation of the total elastic cross sections in a screened Coulomb potential indicates that $\sigma(H^+ + O) \simeq .12\ \text{Å}^2$ and $\sigma(H^+ + C) \simeq .08\ \text{Å}^2$, which are roughly 10% of typical C or O hard sphere cross sections. One may also compare in order of magnitude the collision time $T_c \sim (a_o / v_{H^+}) \simeq 10^{-16}$ sec, where v_{H^+} is the proton velocity and a_o the Bohr radius, with a typical molecular vibration period $T_v \sim 10^{-14}$ sec. Furthermore, a calculation of the displacement of the atom during an H^+ + free-atom collision shows that this displacement is approximately 1% of the interatomic separations in CO_2. Since these considerations all give support to the H^+ + single free-atom impulse approximation, the calculations based on molecular break-up are thought to be the most realistic. (Similar arguments apply to collisions with N_2.)

We now consider what type of cross sections are appropriate to $\begin{pmatrix} H^+ \\ \alpha \end{pmatrix} + \begin{pmatrix} C \\ O \\ N \end{pmatrix}$ collisions, where the latter column refers to molecular constituents. The energies involved here, about 1 keV for the H^+ and 4 keV for the α particles, are such that in a close encounter the ion penetrates appreciably into the electronic cloud of the atom, necessitating the use of a screened Coulomb potential to describe the interaction. Such a potential may be written as

$$V(r) = \frac{Z_1 Z_2 e^2}{r} \Phi\left(\frac{r}{a}\right)$$

where r is the internuclear separation, Z_i is the nuclear charge of species i, and $\Phi\left(\frac{r}{a}\right)$ is a screening function such

that $\Phi \to 1$ for $r << a$ and $\Phi \to 0$ for $r >> a$. A suitable screening function is provided by the Thomas-Fermi model, which gives a scale length or "screening radius," $a = [.8853\, a_o/(Z_1^{2/3} + Z_2^{2/3})^{1/2}]$. One then conventionally defines (Lindhard, et al., 1968) the "reduced energy", ϵ, of the collision to be the ratio of the initial kinetic energy in the center-of-mass system to the Coulomb energy at $r = a$, $\epsilon = (a/Z_1 Z_2 e^2)\ 1/2\ \mu v_{rel}^2$ where $\mu = m_1 m_2/(m_1 + m_2)$ is the reduced mass, and v_{rel} is the relative velocity. We also have $\epsilon = a/b$ where b is the distance of closest approach of the nuclei in a head-on collision. Collisions with $\epsilon << 1$ involve very little penetration of the electronic cloud and are thus well described by hard sphere cross sections. Those having $\epsilon >> 1$, on the other hand, involve a close nuclear encounter, so that screening effects are small and one essentially has Rutherford scattering. In the intermediate case of $\epsilon \simeq 1$, however, it is necessary to make full use of the screened Coulomb potential to describe the collision. For the collisions under consideration, the reduced energies are given in Table I.

These energies fall within the intermediate screening regime. However, use of cross sections calculated from the Thomas-Fermi potential would have necessitated many numerical integrations in the course of the program to determine free path lengths and energy transfers. Consequently, we used instead a potential

$$V(r) = \frac{Z_1 Z_2 e^2}{r}\ \frac{(ka/2)}{r}$$

which approximates the Thomas-Fermi potential for $r \sim a$ and leads to simple analytic expressions for the energy transfer. Here $k = 2.26/\gamma = .831$, with $\gamma = 2.72$ = Euler's constant.

Defining a parameter $t = \epsilon^2 (T/T_m)$, where $T_m = [4m_1 m_2/(m_1 + m_2)^2]E$ is the maximum possible energy transfer, one finds (Lindhard, et al., 1968) a differential cross section $d\sigma/dt = (\pi a^2/2t^{3/2})\ f(t^{1/2})$, where $f(t^{1/2}) = k\pi/8$ for an inverse square potential. Fig. 1, taken from (Lindhard, et al., 1968), gives a comparison of $f(t^{1/2})$ for the Thomas-Fermi and inverse square potentials. The ranges of $t^{1/2}$ relevant to the various collisions are given below in Table II. The minimum energy transfer considered, T_{min}, was the sum of the dissociation energy of the atom and its gravitational potential energy.

For the H^+ collisions the two $f(t^{1/2})$ values differ by as much as 50% (at $T = T_m$), while for the α collisions they differ by up to 65%. The significance of this discrepancy for the determination of cross sections and energy transfers was investigated for the $H^+ + O$ case. Integrating $d\sigma/dt$ between the limits indicated for both the Thomas-Fermi and inverse square potentials, we find $\Delta\sigma/\sigma_2 = (\sigma_{TF} - \sigma_2)/\sigma_2 \simeq .054$ which means that the value for the inverse square cross section σ_2 used in our calculations is $\sim 5.4\%$ too small. For the average energy transfer $\overline{T} = \int T d\sigma/\sigma$ we find $\Delta\overline{T}/\overline{T}_2 \equiv (\overline{T}_{TF} - \overline{T}_2)/\overline{T}_2 \simeq -.13$, so our $\overline{T}_2$ is $\sim 13\%$ too large. Extrapolating from the theory of sputtering of a solid (Sigmund, 1969), we expect that the sputtering yield should be proportional to the stopping power $dE/dx = n\int T d\sigma$. Thus if the results of the collisions $H^+ + C$, etc. are similar to the results

for H^+ + O above, our yields are about 10% larger than would be obtained through use of the true Thomas-Fermi potential. We note that the total H^+ (1 keV) + CO_2 cross section for transferring energy $T \geq T_{min}$ in the inverse square potential approximation, is $\sigma = .314\ \text{Å}^2$. We should also mention that cutting off the energy transfers at T_{min} does not allow $H^+(\alpha)$ deflections through small angles. For H^+ + O the minimum angle is 20^o in the laboratory frame. Such a cutoff is necessary with an inverse square potential to obtain a finite total cross section. It corresponds to the fact that small angle scattering falls off very quickly in the true finite-range atomic potential.

The collisions of the various atoms and molecules recoiling from the primary events discussed above are of a simpler nature. For the C + CO_2 collisions we find (in view of our assumed H^+ + C cross section) that an average C energy is 50 eV (180 eV) for $H^+(\alpha)$ induced cascades. Similarly, for CO_2 + CO_2 we find an average CO_2 energy, resulting from the $H^+(\alpha) \rightarrow C \rightarrow CO_2$ sequence, of 17 eV (60 eV). The corresponding energies for O are even lower, so it would appear that, on the average, hard sphere cross sections are appropriate here. Of course, higher energy transfers are possible with a maximum reduced energy $\epsilon = .2$ for C + CO_2 in α-induced cascades. However, such high energy collisions should be infrequent enough that the hard sphere assumption remains a good one. Hard sphere cross sections were calculated on the basis of the Thomas-Fermi screened Coulomb potential.

The resulting atomic radii were .75 Å, .875 Å, and 1.0 Å for C, N, and O respectively; CO_2 and N_2 radii were taken, conservatively, to correspond to spheres of volume equal to the sum of the volumes of their respective constituents. These choices resulted from the assumption that the interatomic potential energies were on the order of 10 eV at separation distances equal to the sum of the hard sphere radii involved. The resulting hard sphere cross sections, σ_{hs}, are given in Table III.

The thermal kinetic energy of the atmospheric molecules was neglected. A typical atmospheric temperature is 200 ^oK so that 3/2 kT = .026 eV, which is clearly negligible with respect to cascade energies. The variation of the gravitational binding energy with altitude was also neglected since we were concerned with altitude ranges only on the order of 50 km. The escape energy of CO_2 is 5.5 eV, and the corresponding values for C, O, N_2, and N are 1.5 eV, 2.0 eV, 3.5 eV, and 1.75 eV, respectively.

II.

For an atmosphere whose density varies as $\rho(z) = \rho_o e^{-z/H}$ one commonly defines a "critical height," h_c, at which the mean free path of an atmospheric molecule moving in the horizontal plane with a velocity much greater than the mean thermal velocity is just equal to the scale height, H. That is,

$$H = [\sigma \rho_o \exp(-h_c/H)]^{-1}.$$

For our model CO_2 atmosphere, h_c = 171.1 km. Recoiling molecules moving at altitudes $z \gg h_c$ follow ballistic trajectories with relatively little chance of

collision, whereas those moving at $z \ll h_c$ suffer frequent collisions and are quickly thermalized. Consequently, we should expect most sputtering events to originate in a critical layer extending a few scale heights on either side of h_c. We may estimate the lateral dimension of cascades in this critical layer by comparison with the case of a target of uniform density. If we define a cascade to include only those secondaries having energies greater than the minimum energy U necessary for an atom to escape the target, and if $\overline{T}$ is the average energy of the primary initiating the cascade, then a typical cascade radius is $\ell(\overline{T}/U)^{\frac{1}{2}}$, where ℓ is the mean free path of the target atoms. For CO_2 cascades in the critical layer U = 5.5 eV, ℓ = H = 10 km and $\overline{T}$ = 40 eV, which is the average of the C and O primary energies. Thus we expect the lateral extension of the cascade in the horizontal plane to be on the order of 30 km.

A Monte Carlo program was written based upon these considerations and utilizing the cross sections discussed above. Five different runs were made. However, one of these was based on the assumption of no CO_2 break-up and resulted in a sputtering yield S = .0015 which was about an order of magnitude lower than those obtained with the complete break-up assumption. Since it seems that the no-break-up assumption is a poor one, we shall not discuss this case further. The remaining runs will be labeled as: 1) $H^+ + CO_2$, 2) $\alpha + CO_2$, 3) $H^+ + N_2$, 4) $\alpha + N_2$.

The cascades initiated by the incident H^+ and α were calculated separately and consecutively, since they are mutually independent. No collisions were allowed above z = 300 km. For each incident H^+ (or α) a first collision altitude was chosen above $h_c - \Delta z$, where Δz = 25-35 km, depending on the run. That is,

we sampled only that fraction of the total solar wind flux initiating its first cascade in the layer $h_c - \Delta_z < z < 300$ km. This choice was dictated essentially by varying Δz and observing that negligibly few sputtering events were induced by H^+ collisions below the chosen level. Upon each H^+ collision the cascade due to the primary recoil C or O (or N) atom was calculated by making random choices of free path lengths, azimuthal angles φ, and energy transfers. Using hard sphere cross sections, all energy transfers $0 < T < T_m$, were allowed. The technique employed for these choices was as follows: For each variable, x, having an allowed range (a, b) and a probability distribution p(x) on this range, a random number, n, was chosen in the interval (0, 1) and the value of x was determined from

$$n = \int_a^x p(x')\, dx' .$$

If $x = \varphi$, we have a = 0, b = 2π, $p(\varphi) = 1/2\pi$, and thus

$$N = \int_0^{\varphi} \frac{d\varphi'}{2\pi} = \frac{\varphi}{2\pi}$$

or $$\varphi = 2\pi n.$$

Each C, O, or CO_2 was followed until either its energy fell below its escape energy or it moved above 300 km. In the latter case it was recorded as a sputtered particle if its kinetic energy exceeded its escape energy. Subsequent collisions of the same proton were calculated, this time with no lower bound on z. A maximum of 3-7 such collisions, depending on the run, were considered, since subsequent ones produced very few sputtering events.

The validity of this latter procedure was investigated by making a separate calculation of proton paths through the atmosphere. Each H^+ having its first collision between 146 km and 300 km was followed until either it escaped or its energy fell below 200 eV. Of the 50 H^+ considered it was found that 46%

had more than 5 collisions, but that these H^+ were invariably below 146 km by their 5th collision. There was a definite tendency for the proton direction of motion to be reversed near the end of its range. In 10% of the trials, an H^+, having had more than 5 collisions (and having penetrated below 146 km), was found to move back above 146 km and suffer 1 or 2 collisions before escaping. It is also interesting to note that 62% of the H^+ eventually escaped from the atmosphere before their energy fell below 200 eV, and that 36% escaped from (i.e., had their last collision) below 146 km. In view of these results, it seems that our values for the sputtering yields could be on the order of 10% too small as a consequence of the cutoff at 5 collisions. The inefficiency of this procedure is evident in that many cascades are calculated for which the chance of a sputtering event is negligible. A better approach would perhaps be to calculate only those cascades initiated by collisions satisfying certain criteria involving depth in the atmosphere, energy transferred and possibly the direction of recoil. This approach could also account for those H^+ which have their first collision deep in the atmosphere but eventually rebound above 146 km and initiate cascades, a possibility which is not considered in the present program.

Table IV summarizes some of the important parameters which varied from run to run. The atmospheric model used in runs 3 and 4 included only the N_2 component. However, since we do not expect sputtering yields to depend strongly on the magnitude of the target density (see below), a model which included both the CO_2 and N_2 components should produce results which differ from ours primarily as a consequence of the dilution of the N_2 by the CO_2 in the critical layer. At altitudes near 170 km the Martian atmosphere is $\sim 10\%$ N_2

(Nier and McElroy, 1976; Nier and McElroy, 1977), so that the sputtering yields quoted below for runs 3 and 4 are about an order of magnitude higher than would be obtained from such a two component model. There will, in addition, be smaller second order effects due to the variation of the relative concentrations of CO_2 and N_2 with altitude, the difference in energy transfer efficiencies between $N_2 + N_2$ and $N_2 + CO_2$ collisions, etc. These considerations are investigated in more detail in Section IV.

Output from the program was generated at each sputtering event. This information included the species of the sputtered particle, the position of its last collision, its energy and angle of emission. The altitude of the $H^+ + CO_2$ collision giving rise to this event was recorded, as was the number of collisions the proton in question had suffered up to this point. The sputtering yield, S, for a given species is defined as the ratio of the number N, of atoms or molecules of that species which escape the atmosphere to the total number of incident particles, D. As mentioned above, we required each particle to have its first collision in the critical layer. If f is the probability that a particle incident at 300 km will have a collision before reaching $h_c - \Delta z$, then D is determined from our sample size, F, by $F = fD$. F is the number of distinct H^+ or α particles for which cascades were calculated. The value of f was calculated for each run and is given in Table IV. The sputtering yields, $S \equiv N/D = fN/F$, obtained for each of our calculations are presented in Table V.

The relative importance of these yields may be judged by noting that typical H^+ and α fluxes in the vicinity of Mars are $9.5 \times 10^7/cm^2$-sec and $5 \times 10^6/cm^2$-sec respectively (Brandt, 1970) implying roughly equivalent rates of H^+ and α induced sputtering. Although no detailed comparison has been made,

we note that these yields seem to be of the same order of magnitude as the corresponding values for the sputtering of a solid, based on Sigmund's theory (Sigmund, 1969). As an example, we compare the results of run 1 with the prediction of the theory for 1 keV protons incident on a random target of average atomic number $\overline{Z} = 7.3$, average atomic weight $\overline{A} = 14.6$, and average surface (chemical) binding energy $\overline{U} = 1.8$ eV. The appropriate screening radius is $a = .215\ \mathring{A}$ and the reduced energy is $\epsilon = 1.91$, so that the predicted sputtering yield is S (1 keV) = .19. This should be compared to the effective yield of atoms implied by run 1, i.e. $S_{eff} = 3\,S_{CO_2} + S_C + S_O = .055$. The fact that theory and calculation produce similar results here is not surprising considering that Sigmund treats a random solid essentially as if it were a dense gas, ignoring any bulk, or lattice, binding energy. The density, ρ, of the target enters the calculation of the sputtering yield in two mutually compensating ways. On one hand, the number of secondaries formed per unit volume per unit time is directly proportional to ρ, while on the other hand the probability that a secondary of given energy will reach the target surface without collision, integrated over the target volume, is inversely proportional to ρ. Since these two factors cancel each other, the sputtering yield is found to be independent of ρ, at least for a target of uniform density. Consequently, neglecting bulk binding energies and target non-uniformities, one expects similar yields within the framework of this model for solids and gases.

This statement is true for low-energy collisions as long as the separation of the atomic centers exceeds some critical distance whose order of magnitude is an atomic diameter. For solids this criterion is generally not satisfied very

well, and the model described in this paper and in (Sigmund, 1969) may be inadequate. Put another way, the conventional sputtering theory of solids is more appropriate when applied to the problem of the dilute gas target considered here than when applied to the problem for which it was constructed!

Figures 2 - 6 present an analysis of the output from run 1. They include data for all sputtering events, not just CO_2. Fig. 2 shows the lateral position of the last collision suffered by a sputtered particle prior to leaving the atmosphere. The protons are all incident at the point (0,0). Nearly all sputtered molecules originate within ~ 50 km of the initial H^+-molecule impact, in the lateral dimension, and the width of a typical cascade is perhaps 60 km, which agrees with our earlier estimate.

Fig. 3 provides similar information on the vertical extent of the cascade, but in histogram form. The distribution is centered around the critical height h_c, as expected, with a full width of perhaps 40 km. The distribution is not symmetrical, as in Fig. 2, presumably in part because of the changing atmosphere density with altitude.

Fig. 4 indicates that the distribution in altitude of the primary collisions is somewhat narrower and lower than that of the sputtered particles. This is consistent with the fact that secondaries escape preferentially from higher altitudes. The distribution in this figure, as well as that of the sputtered particles in Fig. 3, would appear quite sharp were it not for the suppressed zeroes. This points up the fact that as far as sputtering is concerned, the top of the atmosphere provides a reasonably sharp boundary.

It is interesting to compare the energy and angle distributions of Figs. 5

and 6 with those derived from the sputtering theory of solids (Sigmund, 1969). We assume (Thompson, 1968; Weller, 1973) that the energy spectrum within the solid is proportional to $1/E'^2$ and that the velocity distribution of recoiling atoms is isotropic. Then the flux of secondaries with energy in dE' about E' and velocity vector $\vec{v}'$ in the solid angle interval $d\Omega'$ about Ω', through a surface whose normal makes an angle θ' with $\vec{v}'$, has the form (Thompson, 1968)

$$\Phi(E', \Omega')\ d\Omega' dE' \propto \frac{dE'}{E'^2}\ \frac{d\Omega'}{4\pi}\ \cos\theta'.$$

Since an atom with energy E' greater than some minimum value U will escape the surface if its velocity is directed in the outer hemisphere, the conversion to an asymptotic sputtered flux is made by taking $E' = E + U$ and $\Omega = \Omega'$, so that

$$\Phi(E,\Omega)\ d\Omega dE \propto \frac{dE}{(E+U)^2}\ \frac{d\Omega}{4\pi}\ \cos\theta.$$

Here θ is the polar angle with respect to the normal to the target surface. We find that the spectrum of Fig. 5 follows $1/(E+U)^2$ fairly well with U between 3.5 and 4.0 eV. The (average) gravitational binding energy for all particles considered here is 3.7 eV.

The angular distribution of Fig. 6 indicates that there is a depletion of the flux at small angles when compared to the above cos θ dependence. $\theta = 0$ is upward from the planetary surface, or backward relative to the solar wind flux. This indicates that, in fact, the flux of secondaries in the cascades is not isotropic.

What are the implications of sputtering for atmospheric mass loss? If φ is the solar wind proton flux, then the CO_2 loss rate is $R = \varphi S_{CO_2}$. We base our estimate of φ on the observed mean proton density in the vicinity of the

earth (Brandt, 1970), $\rho \sim 5/cm^3$, with a velocity $V_{H^+} = 4.38 \times 10^7$ cm/sec corresponding to 1 keV. This gives a flux at Mars of $\varphi = 9.5 \times 10^7/cm^2$-sec. The following loss rates include the effects of both H^+ and α sputtering with an assumed α flux equal to $5 \times 10^6/cm^2$-sec, i.e., 5% of the total flux (Brandt, 1970),

$$R_{CO_2} = 2.6 \times 10^6/cm^2\text{-sec},$$

$$R_O = 7.7 \times 10^5/cm^2\text{-sec},$$

$$R_C = 6.6 \times 10^5/cm^2\text{-sec}.$$

Together, these rates give a mass loss rate equivalent to a CO_2 loss rate of: $R_{equiv.} = 3 \times 10^6/cm^2$-sec. Multiplying $R_{equiv.}$ by the age and illuminated surface area of the planet, one finds a total loss of $\sim 10^{41}$ molecules, roughly the number of CO_2 molecules in the Martian atmosphere today.

A more important measure of the significance of these rates is to compare them with the loss rates estimated for other mechanisms. McElroy (McElroy, 1972; McElroy, et al., 1977) has calculated loss rates for C and O atoms due to chemical and photochemical processes in the Martian atmosphere. We list below the important reactions and associated loss rates.

Oxygen:
$$\left.\begin{aligned} &CO_2^+ + O \rightarrow O_2^+ + CO \\ &O_2^+ + e \rightarrow O + O \\ &CO_2^+ + e \rightarrow CO + O \end{aligned}\right\} \quad P_O = 6 \times 10^7/cm^2\text{-sec}$$

Carbon:
$$CO^+ + e \rightarrow C + O \qquad P_C = 1.5 \times 10^5/cm^2\text{-sec}$$

$$\left.\begin{aligned} h\nu + CO_2 &\rightarrow C + O + O \\ h\nu + CO &\rightarrow C + O \\ e + CO_2 &\rightarrow e + C + O + O \\ e + CO &\rightarrow e + C + O \end{aligned}\right\} R_C = 6 \times 10^5/cm^2\text{-sec}$$

$$e + CO_2^+ \rightarrow C + O_2 \qquad R_C \leq 4 \times 10^5/cm^2\text{-sec}$$

In addition, a loss rate (McElroy, 1972; McElroy, et al., 1977) for CO_2 as large as $5 \times 10^5/cm^2$-sec may result from the electromagnetic interaction of CO_2^+ with the solar wind.

According to these numbers, the dominant mass loss mechanism is chemical ejection of oxygen atoms. The total mass loss due to sputtering amounts to about 10% of the loss due to these other mechanisms. However, the single most important exospheric sink for carbon is due to solar wind sputtering. The existence of this previously unstudied process may have a bearing on our understanding of the Martian CO_2/H_2O ratio (Mutch, et al., 1976).

Because both the process of cascade initiation and that of sputter ejection are surface and mass sensitive, large chemical and isotopic fractionation effects are possible, and these are discussed in the next section.

IV

We have seen that solar wind sputtering is a phenomenon associated with the critical layer in the upper atmosphere. Consequently, the loss rates for the

various species present in the atmosphere should reflect their concentrations in this critical layer, and not their total abundances. For instance, since the Viking data (Nier and McElroy, 1976, 1977; Nier et al., 1976a; Owen and Biemann, 1976; Owen et al., 1977) show that the mixing ratio of N_2 to CO_2 is much greater at altitudes near 170 km than for the bulk atmosphere we should expect the N_2 to be sputtered preferentially. Furthermore, since cascade recoil kinematics depend on the recoil-particle mass, the stoichiometry of the material sputtered is not necessarily identical to that of the critical layer. An analytical study (Watson and Haff, 1978) indicates, however, that the differences in the energy spectra of the recoiling species are likely to result in only small departures from the stoichiometry of the critical layer. The largest effect is due instead to differences between the gravitational potential energies, U_i, of the species. If S_i is the sputtering yield, $n_i^{(c)}$ the density in the critical layer, and m_i the mass of species i, we find that to a good approximation,

$$S_i/S_j = U_j n_i^{(c)}/U_i n_j^{(c)} = m_j n_i^{(c)}/m_i n_j^{(c)} \quad . \qquad (1)$$

All these considerations apply equally well to the case of isotopes.

The implications of the foregoing effects for the history of the Martian atmosphere have been investigated by considering a model atmosphere, with a present composition of 2.5% N_2 (Nier, et al., 1967a; Owen and Biemann, 1976; Owen, et al., 1977) and 97.5% CO_2, assumed to have been rapidly out-gassed 4.5×10^9 years ago. We assume a subsequent passive role for the surface and consider only that mass loss which is due to sputtering by a constant solar wind flux, Φ. Let $n_i(t)$ and $n_i^c(t)$ be the column densities (molecules/cm^2) of species i for the bulk

atmosphere and critical layer respectively at a time t (the atmosphere being formed at t = 0). The corresponding mixing ratios of N_2 to CO_2 are given by

$$f(t) = n_{N_2}(t)/n_{CO_2}(t)$$

and

$$f_c(t) = n^{(c)}_{N_2}(t)/n^{(c)}_{CO_2}(t).$$

The parameter $R \equiv f_c(t)/f(t)$ (McElroy and Yung, 1976; Nier, et al., 1976b) is then a measure of the enrichment of the critical layer in thelighter species due to diffusive separation. The dynamics of the atmosphere are assumed to be such as to maintain R essentially constant in time. With reference to the Viking data (Nier and McElroy, 1976, 1977; Nier, et al., 1976a; Owen and Biemann, 1976; Owen, et al., 1977) we estimate R = 5.5, and we take $n(T) \equiv n_{CO_2}(T) + n_{N_2}(T) = 2.7 \times 10^{23}$ molecules/cm^2 where $T = 4.5 \times 10^9$ y. The sputtering yield of CO_2 is determined by

$$S_{CO_2}(t) = S n^{(c)}_{CO_2}(t)/(n^{(c)}_{CO_2}(t) + n^{(c)}_{N_2}(t)) = S/(1 + Rf(t)), \qquad (2)$$

where S is the result of our numerical calculation for an atmosphere of pure CO_2 and is constant in time. We use the molecular equivalent of the total mass loss per incident H^+, S = .018 and we account for the α-component of the solar wind by taking $\varphi = 2 \times 10^8$ cm^{-2}sec^{-1}. The sputtering yield for N_2 is given, using Eq. (1), by

$$S_{N_2}(t)/S_{CO_2}(t) = m_{CO_2} n^{(c)}_{N_2}(t)/(m_{N_2} n^{(c)}_{CO_2}(t)) = Rf(t) m_{CO_2}/m_{N_2}. \qquad (3)$$

The equations governing the evolution of the sputtered atmosphere are then,

$$dn_{N_2}(t)/dt = -S_{N_2}(t)\varphi/2$$

and

$$dn_{CO_2}(t)/dt = -S_{CO_2}(t)\varphi/2 \qquad (4)$$

The factor of 1/2 crudely reflects the fact that only half the surface area is illuminated at any given time. The following relations derive from Eqs. (2-4),

$$n_{N_2}(t)/n_{N_2}(0) = \left[n_{CO_2}(t)/n_{CO_2}(0)\right]^{R(m_{CO_2}/m_{N_2})} \qquad (5)$$

and

$$n_{CO_2}(t) - n_{CO_2}(0) + \left[n_{N_2}(t) - n_{N_2}(0)\right](m_{N_2}/m_{CO_2}) = -S\varphi t/2. \qquad (6)$$

The initial composition of the atmosphere may be determined by simultaneous solution of Eqs. (5) and (6), with the results

$$n_{CO_2}(0) = 1.46\, n_{TOT}(T) = 3.94 \times 10^{23}\ \text{cm}^{-2},$$

and

$$n_{N_2}(0) = 0.80\, n_{TOT}(T) = 2.16 \times 10^{23}\ \text{cm}^{-2},$$

$$n_{TOT}(0) = 2.26\, n_{TOT}(T) = 6.10 \times 10^{23}\ \text{cm}^{-2},$$

where $n_{TOT}(T)$ is the total column density of the bulk atmosphere at time $T = 4.5 \times 10^9$ y. Thus, this model implies that the initial Martian atmosphere was 35% N_2 and 65% CO_2. In the course of 4.5×10^9 y about 56% of these molecules have been lost. Over the same period roughly 33% of the CO_2 and 97% of the N_2 has been sputtered away. A calculated N_2 depletion of 97% through sputtering is similar to mass loss estimates based on other mechanisms (Nier, et al., 1976b; McElroy, et al., 1976; Brinkman, 1971) (e.g. photochemical reactions), and it is clear that sputtering effects

must be considered in any realistic model of atmospheric evolution..

Given the above results we may make a similar analysis to determine the enrichment expected among nitrogen isotopes if the initial ratio of ^{15}N to ^{14}N equalled its present terrestrial value, $^{15}N/^{14}N = .00368$. The value of the parameter R is determined (McElroy, et al., 1977) to be

$$R = n_{28}^{(c)}(t)n_{29}(t)/(n_{29}^{(c)}(t)\, n_{28}(t)) = 1.14,$$

where the subscripts designate the isotopic composition of the molecule. Then, bearing in mind that nitrogen is lost mainly in molecular form, we find

$$n_{28}(t)/n_{28}(0) = [n_{29}(t)/n_{29}(0)]^{R(29/28)},$$

analagous to equation (5). From this we derive the expected present column densities:

$$n_{28}(T) = .0247\, n_{TOT}(T) = 6.67 \times 10^{21} cm^{-2},$$

$$n_{29}(T) = .0003\, n_{TOT}(T) = 0.81 \times 10^{20} cm^{-2}.$$

These in turn imply:

$$n_{14}(T) = 1.34 \times 10^{22} cm^{-2},$$

$$n_{15}(T) = 0.81 \times 10^{20} cm^{-2}.$$

The enrichment of ^{15}N in the present atmosphere, compared with the initial $^{15}N/^{14}N$ ratio, taken here to be the same as its present terrestrial value, may be measured by the quantity (Nier, et al., 1976b)

$$\epsilon_N(T) \equiv n_{15}(T)\, n_{14}(0)/(n_{14}(T)\, n_{15}(0)).$$

For the model discussed here $\epsilon_N(T) = 1.7$, while the enrichment observed by the Viking lander (Nier, et al., 1976b; Biemann, et al., 1976; Owen, et al., 1977)is ≤ 1.75. The fractionation effects induced by solar wind sputtering are therefore very likely to be of the same order of magnitude as observed effects, and in detailed evolutionary studies of the Martian atmosphere they will have to be taken into account.

Of course in the sputtering process, as in other processes leading to ballistic ejection of atoms or molecules, other sets of atmospheric isotopes also suffer a large fractionation. Thus, when the above equations are applied to the $^{13}C/^{12}C$ ratio we find $\epsilon_C(T) = 1.05$ which may be compared to the observed limit (Nier, et al., 1976b; Biemann, et al., 1976; Owen, et al , 1977; Nier and McElroy, 1977) $\epsilon_C(T) \leq 1.05$. As stated, there is some selectivity in fractionating nitrogen preferentially, both because of the lower gravitational binding energy of the N_2 molecule compared to the CO_2 molecule (in which the C atoms reside) and because its density distribution does not drop off as quickly with altitude. But these effects cannot explain why it is nitrogen alone which shows such large fractionation. The source of such differences will have to be sought in a different direction entirely, perhaps with an eye to the role of the Martian crust as a carbon and oxygen reservoir.

APPENDIX

We discuss here the statistical reliability of our results. Consider the case of $S_{tot} \equiv S_{CO_2} + S_C + S_O$ for run 1. We assume that the outcome of our calculations is well characterized by a multinomial distribution. That is, for each incident H^+ we assume a certain probability p_n that n particles will escape ($n = 0, 1, 2, \ldots$), and we take p_n to be the ratio of the number of such events observed to the total number of incident particles (the sample size, F). The standard deviation in the number of particles observed is then easily calculated (Hogg and Craig, 1970). If, in addition, we take account of the error implicit in the assumption that the incident dose is given by $F = fD$, then we find a statistical error of 10% in S_{tot}. This is certainly no larger than the errors introduced by other assumptions of our model; consequently, it does not seem profitable to increase the sample size in our present program unless substantial progress is made in removing the major uncertainties.

As a general check on the reliability of the computer program, it was adapted to the sputtering of a solid surface for which we have experimental values for the sputtering yields. The most important changes involved in this adaptation were a consequence of the change from an exponentially varying target density to a uniform one. Another important modification was the change from a spherical potential barrier at the top of the atmosphere to a work-function boundary at the solid surface. An inverse square screened Coulomb potential was used to describe collisions above certain critical energies while hard sphere cross sections were assumed at smaller energies. We should also mention that

all ion-target collisions were considered which were close enough to the surface to result in a sputtering event. This differed from the atmospheric case in that only five $H^+ + CO_2$ collisions were considered in the latter. These modifications involved substantial changes in the equations used to determine the position of collisions and the escape criteria, but the basic mechanics of the program were otherwise left unaltered. We considered the case of Kr incident on Cu at two different energies with the following results:

$S_{Cu} \simeq 10$	E = 100 keV	Dose = 40
$S_{Cu} \simeq 4$	E = 1 keV	Dose = 10

These sputtering yields are both within a factor of 2 of the experimental values: S_{Cu} (100 keV) ≃ 13, S_{Cu} (1 MeV) ≃ 7.5 (Sigmund, 1969). Given the input assumptions of our model, this agreement is about as close as could be expected. Consequently, we conclude that our program provides a reasonable simulation of the physical process.

Another point not yet discussed is the assumed independence of the cascades. An estimate of the probability that one secondary would strike another energetic CO_2 moving in the same or an overlapping cascade might be made by taking the ratio of the number of CO_2 secondaries in the cascade volume to the total number of molecules present in that volume. Let us consider the volume 160 km ≤ z ≤ 190 km with a radius of 30 km in the horizontal plane. Suppose that each cascade generates 100 secondaries with energies > 5.5 eV (a high estimate), and that the number of cascades initiated per cm^2 per sec is φf, where $\varphi = H^+$ flux at Mars and $f \simeq .157$ is the fraction of φ having its initial collision above 146 km. Further suppose that each cascade lasts a time equal

to that required for a 6 eV CO_2 to travel 30 km; t ~ 1 sec. Then we may estimate the above probability to be:

$$p = \frac{\varphi \, ft \, (100)}{\int_{160}^{190} \rho_o e^{-z/H} \, dz} \simeq 2 \times 10^{-9}$$

Since this value must be an upper bound on p, at least for the region of the atmosphere in which most sputtering events occur, we conclude that the cascades are independent.

The final correction to the sputtering yields we have considered is that due to the loss of energy to recoil and excitation processes in $H^+ + CO_2$ collisions. We first note that it is not sufficient to require that the energy transfer to the C or O atom, T, be greater than its dissociation energy, D. Instead one should demand that the relative energy of the two pieces of the molecule in the center-of-mass frame be $\geq$ D, i.e., $1/2 \, \mu v_{rel}^2 \geq D$ or $T \geq m/\mu D$, where m is the C or O mass and μ is the reduced mass of $C + O_2$ or $O + CO$. We find,

$$T_C \geq 15 \text{ eV}$$

$$T_O \geq 8.6 \text{ eV}$$

whereas the minimum energy transfers allowed in our program were:

$$T_C \geq 12.5 \text{ eV}$$

$$T_O \geq 7.5 \text{ eV}$$

This difference should not be very important considering the already approximate nature of our cross sections. A more significant problem is that of the recoil energy of the CO or O_2. We have calculated this recoil energy assuming that the two pieces move away from each other with no relative angular momentum. If E_f = final kinetic energy of the C or O, then we find that to second order in D/T,

$$E_f = T \left\{ 1 - (D/T) \left[1 + (1 + m/\mu)/(D/4T) \right] \right\}$$

For $T \gg D$ we have

$$E_f = T - D$$

which is the equation used in our program. But for $T \sim D$ we find recoil energies on the order of 2–4 eV. This is on the same order as the energy we might estimate to be lost through excitation, ionization, etc. in a typical $H^+ + CO_2$ collision. So if an average cascade energy, ignoring recoil and excitation, is 50 eV, then the above estimates imply as an upper limit, a correction of ~ 20%. The number of secondaries per cascade and consequently the sputtering yield would be reduced by the same amount.

In conclusion we may summarize the four corrections to S we have estimated. The five collision cutoff implied a correction of + 10%. The comparison of the Thomas-Fermi to the $1/r^2$ cross sections gave a correction of -10%. The assumption of a 100% CO_2 atmosphere implied a decrease of ~ 10% in the yield, while the above energy transfer efficiency factor was, at the very most, -20%. Thus, the largest possible correction to our computed value of S due to the above effects would be to reduce it by ~30%.

ACKNOWLEDGEMENTS

We would like to thank Professors D.A. Bromley, D.S. Burnett and T. A. Tombrello for helpful discussions and comments.

REFERENCES

Biemann, K., Owen, T., Rushneck, D.R., LaFleur, A.L., and Howarth, D.W. (1976). The Atmosphere of Mars Near the Surface: Isotope Ratios and Upper Limits on Noble Gases. Science 194, 76-78.

Brandt, J.C. (1970). Introduction to the Solar Wind. W.H. Freeman and Co., San Francisco.

Brinkmann, R.T. (1971). Mars: Has Nitrogen Escaped? Science 174, 944-945.

Haff, P.K., Switkowski, Z.E., and Tombrello, T.A. (1978). Solar-wind Sputtering of the Martian Atmosphere. Nature 272, 803-804.

Hogg, R.V., and Craig, A.T. (1970). Introduction to Mathematical Statistics. MacMillan Co., New York.

Lindhard, J., Nielsen, V., and Scharff, M. (1968). Approximation Methods in Classical Scattering by Screened Coulomb Fields. Kgl. Danske Vidensk. Selskab, Mat.-Fys. Medd. 36, no. 10.

McElroy, M.B. (1972). Mars, An Evolving Atmosphere. Science 175, 443-445.

McElroy, M.B., Yung, Y.L., and Nier, A.O. (1976). Isotopic Composition of Nitrogen: Implications for the Past History of Mars' Atmosphere. Science 194, 70-72.

McElroy, M.B., and Yung, Y.L. (1976). Oxygen Isotopes in the Martian Atmosphere: Implications for the Evolution of Volatiles. Planet. Space Sci. 24, 1107-1113.

McElroy, M.B., Kong, T.Y., and Yung, Y.L. (1977). Photochemistry and Evolution of Mars' Atmosphere: A Viking Perspective. J. Geophys. Res. 82, 4379-4388

Mutch, T.A., Arvidson, R.E., Head, J.W., III, Jones, K.L., and Saunders, R.S., The Geology of Mars, p 283, Princeton University Press, Princeton, 1976.

Nier, A.O., Hanson, W.B., Seiff, A., McElroy, M.B., Spencer, N.W., Duckett, R.J., Knight, T.C.D., and Cook, W.S. (1976a). Composition and Structure of the Martian Atmosphere: Preliminary Results from Viking 1. Science 193, 786-788.

Nier, A.O., McElroy, M.B., and Yung, Y.L. (1976b). Isotopic Composition of the Martian Atmosphere. Science 194, 68-70.

Nier, A.O., and McElroy, M.B. (1976). Structure of the Neutral Upper Atmosphere of Mars: Results from Viking 1 and Viking 2. Science 194, 1298-1300.

Nier, A.O., and McElroy, M.B. (1977). Composition and Structure of Mars' Upper Atmosphere; Results From the Neutral Mass Spectrometers on Viking 1 and 2. J. Geophys. Res. 82, 4341-4349.

Owen, T., and Biemann, K. (1976). Composition of the Atmosphere at the Surface of Mars: Detection of Argon-36 and Preliminary Analysis. Science 193, 801-803.

Owen, T., Biemann, K., Rushneck, D.R., Biller, J.E., Howarth, D.W., and Lafleur, A.L. (1977). The Composition of the Atmosphere at the Surface of Mars. J. Geophys. Res. 82, 4635-4639.

Sigmund, P. (1969). Theory of Sputtering. I. Sputtering Yield of Amorphous and Polycrystalline Targets. Phys. Rev. 184, 383-416.

Spreiter, J.R., Summers, A.L., and Rizzi, A.W. (1970). Solar Wind Flow Past Nonmagnetic Planets - Venus and Mars. Planet. Space Sci. 18, 1281-1299.

Thompson, M.W. (1968). II. The Energy Spectrum of Ejected Atoms During the High Energy Sputtering of Gold. Phil. Mag. 18, 377-414.

Watson, C.C., and Haff, P.K. (1978). Unpublished.

Weller, R.A. (1978). The Energy Spectra of Uranium Atoms Sputtered from Uranium Metal and Uranium Oxide Targets. Thesis. 1978. Unpublished.

TABLE I. Reduced energy ϵ for proton and α-particle collisions.

	ϵ		ϵ
$H^+ + C$	2.41	$\alpha + C$	3.68
$H^+ + N$	2.0	$\alpha + N$	3.15
$H^+ + O$	1.71	$\alpha + O$	2.75

TABLE II. Range of energy transfer parameter for various collision processes.

		T_{min} (eV)	T_m (eV)	
1 keV	$H^+ + C$	12.5	284.	$.506 < t^{1/2} < 2.41$
	$H^+ + N$	11.5	249.	$.430 < t^{1/2} < 2.0$
	$H^+ + O$	7.5	221.	$.315 < t^{1/2} < 1.71$
4 keV	$\alpha + C$	12.5	3000.	$.238 < t^{1/2} < 3.68$
	$\alpha + N$	11.5	2765.	$.204 < t^{1/2} < 3.15$
	$\alpha + O$	7.5	2560.	$.149 < t^{1/2} < 2.75$

TABLE III. Effective hard sphere cross-sections σ_{hs} employed for molecular collisions.

	σ_{hs} ($\AA^2$)
$CO_2 + CO_2$	22.5
$C + CO_2$	13.7
$O + CO_2$	17.2
$N_2 + N_2$	15.27
$N + N_2$	12.29

TABLE IV. Variable Parameters

	$H^+ + CO_2$	$\alpha + CO_2$	$H^+ + N_2$	$\alpha + N_2$
ρ_o	$1.2 \times 10^{16}/cm^3$	$1.2 \times 10^{16}/cm^3$	$4.6 \times 10^{12}/cm^3$	$4.6 \times 10^{12}/cm^3$
H	10.0 km	10.0 km	15.35 km	15.35 km
h_c	171.1 km	171.1 km	142.5 km	142.5 km
F	1000	150	500	150
f	0.157	0.313	0.078	0.223
Critical Layer	146-300 km	146-300 km	112.5-300 km	107.5-300 km
# Collisions Allowed	5	7	5	3

ρ_o = Density constant determined by fitting $\rho(z) = \rho_o e^{-z/H}$ to observed densities in critical layer.

H = Scale height, similarly determined.

h_c = Critical height, calculated from ρ_o, H and the appropriate cross section.

F = Sample size, the number of distinct H^+ or α for which calculations were made.

f = Fraction of the incident dose constituted by F.

Critical Layer = Layer in which the first primary collision was required to occur.

Collisions Allowed = Maximum number of collisions of a single H^+ or α considered.

TABLE V. H^+ and α sputtering yields for pure CO_2 or pure N_2 atmospheres.

	1) $H^+ + CO_2$	2) $\alpha + CO_2$		3) $H^+ + N_2$	4) $\alpha + N_2$
S_{CO_2}	0.014	0.26	S_{N_2}	0.022	0.22
S_C	0.0064	0.010	S_N	0.0056	0.018
S_O	0.0068	0.025			

FIGURE CAPTIONS

Fig. 1. Graph of the reduced differential cross section, $f(t^{1/2}) = \frac{1}{\pi a^2} 2t^{3/2} \frac{dh}{dt}$, for various potentials. $t^{1/2} = \epsilon \{ T/T_m \}^{1/2}$.

Fig. 2. Plot of the x-y coordinates of the last collision of each sputtered particle before leaving the atmosphere.

Fig. 3. Histogram of the z-coordinate (altitude) of the last collision of each sputtered particle before leaving the atmosphere.

Fig. 4. Histogram of primary events ($H^+ + CO_2$) giving rise ultimately to at least one sputtered particle.

Fig. 5. Histogram of the number of sputtered particles at $z = +\infty$ as function of their energy (2.5 eV bins).

Fig. 6. Histogram of the number of sputtered particles per unit solid angle emitted in each 5^o angle interval. $\theta = 0$ corresponds to upward emission.

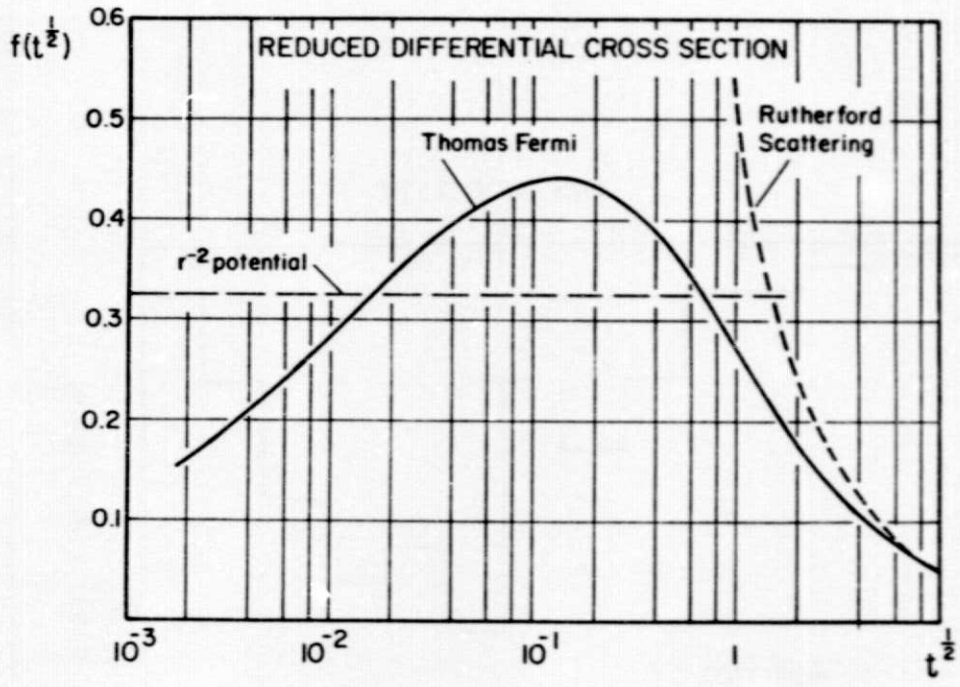

Fig. 1

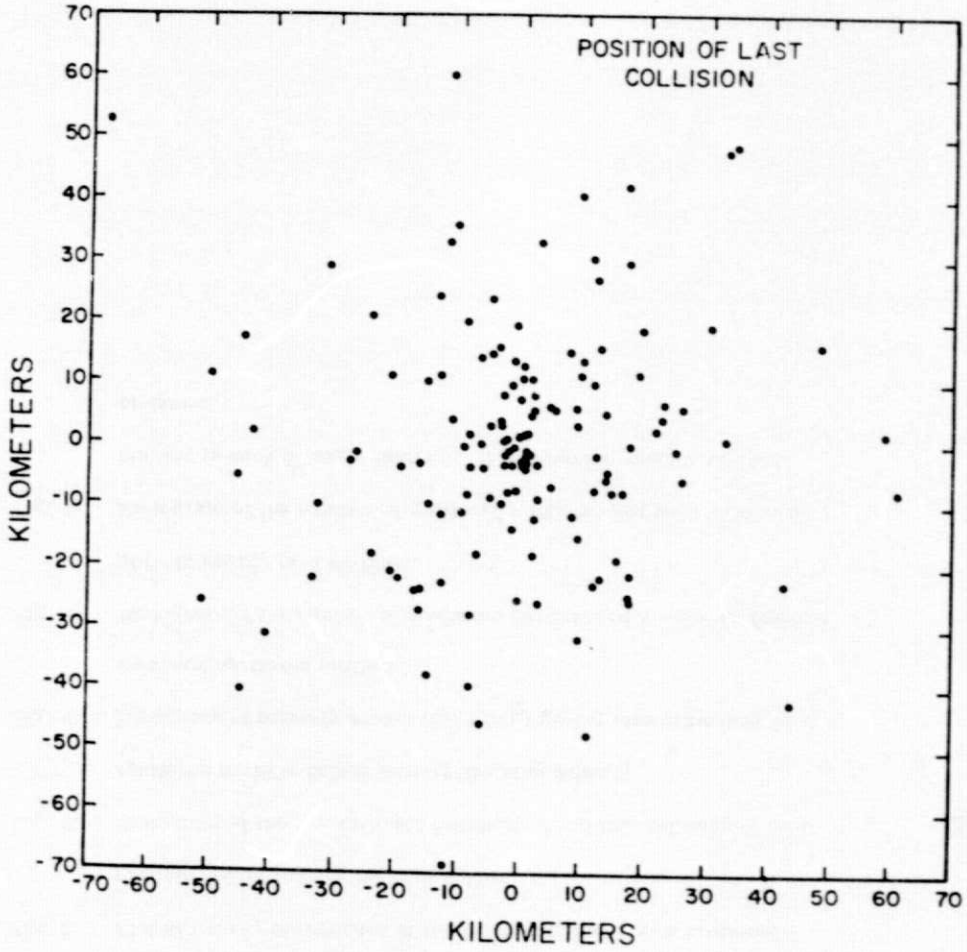
POSITION OF LAST
COLLISION
KILOMETERS
KILOMETERS
70
60
50
40
30
20
10
0
-10
-20
-30
-40
-50
-60
-70
-70 -60 -50 -40 -30 -20 -10 0 10 20 30 40 50 60 70

Fig. 2

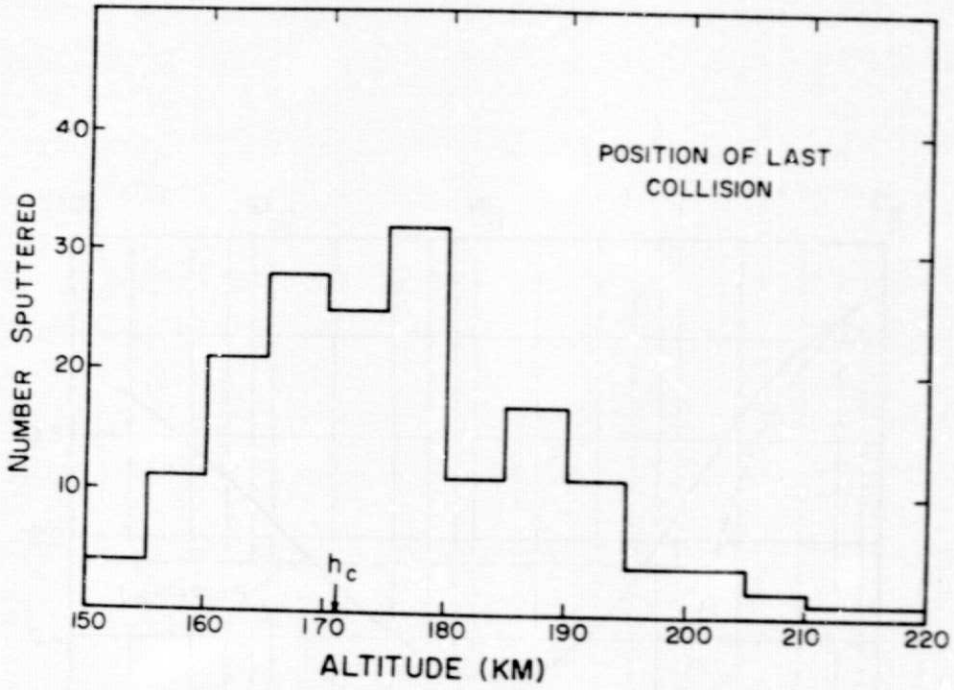
POSITION OF LAST
COLLISION
NUMBER SPUTTERED
40
30
20
10
h_c
150 160 170 180 190 200 210 220
ALTITUDE (KM)

Fig. 3

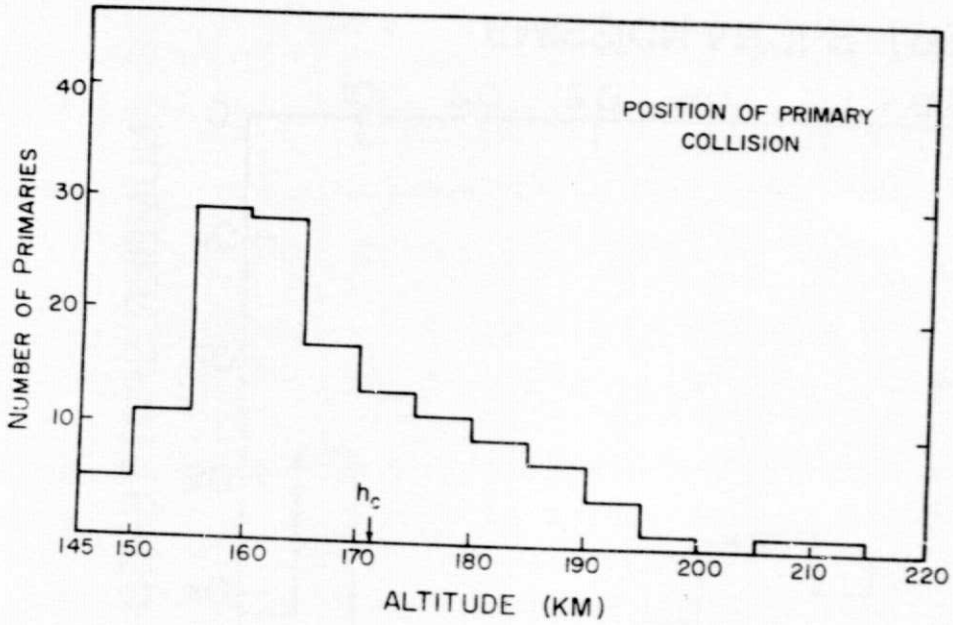
POSITION OF PRIMARY
COLLISION
NUMBER OF PRIMARIES
40
30
20
10
h_c
145
150
160
170
180
190
200
210
220
ALTITUDE (KM)

Fig. 4

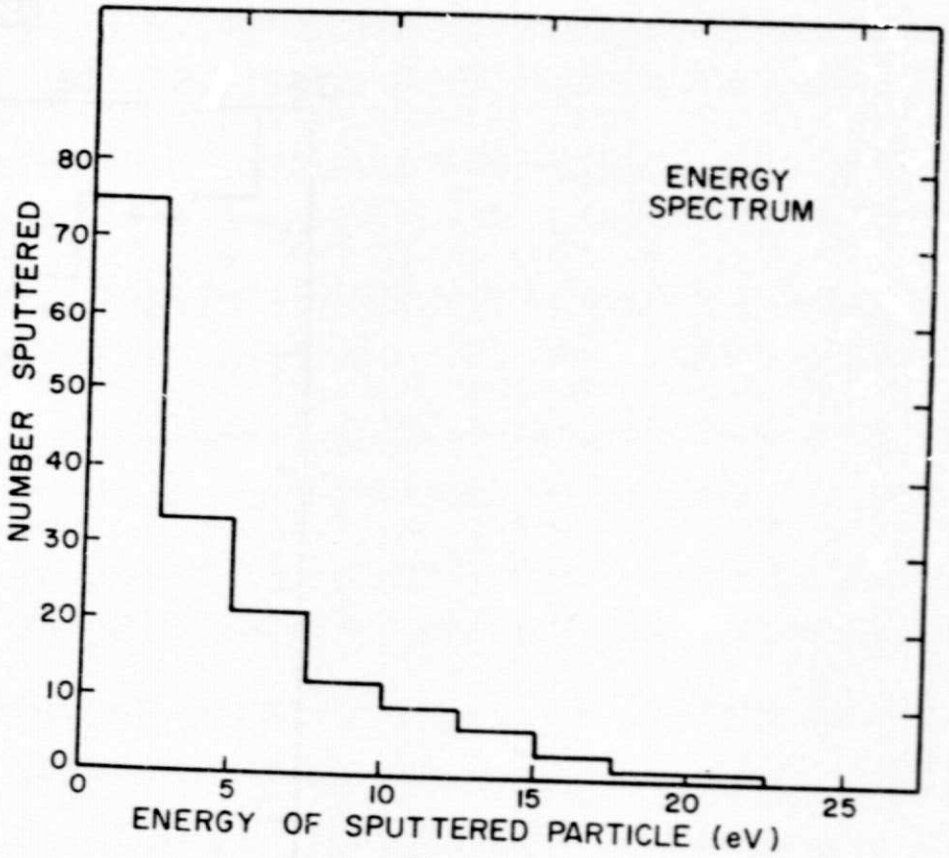
ENERGY
SPECTRUM
NUMBER SPUTTERED
80
70
60
50
40
30
20
10
0
0
5
10
15
20
25
ENERGY OF SPUTTERED PARTICLE (eV)

Fig. 5

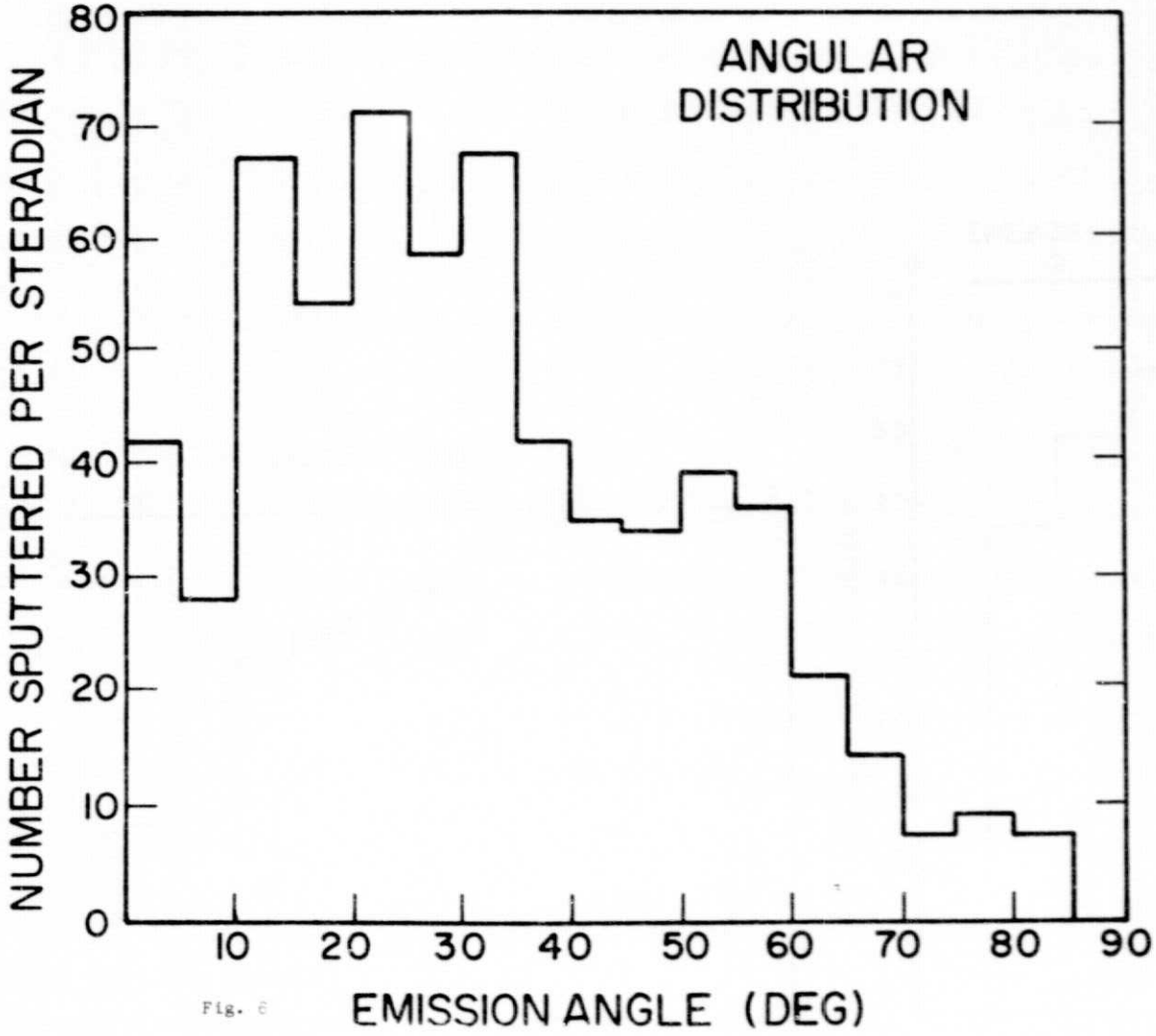
ANGULAR
DISTRIBUTION
NUMBER SPUTTERED PER STERADIAN
0
10
20
30
40
50
60
70
80
10
20
30
40
50
60
70
80
90
EMISSION ANGLE (DEG)

Fig. 6